J Mater Sci: Mater Electron (2014) 25:1547–1552
DOI 10.1007/s10854-014-1766-9

Dielectric response of Sb-doped $CaCu_3Ti_4O_{12}$ ceramics

Yang Liu · Qingrun Chen · Xuguang Zhao

Received: 23 December 2013 / Accepted: 23 January 2014 / Published online: 31 January 2014

Abstract A series of Sb-doped $CaCu_3Ti_4O_{12}$ ceramics were fabricated by the conventional solid state method, and their crystalline structures, microstructures and dielectric properties were investigated systematically. All the ceramic samples exhibited perovskite-related structures in space group $Im\ \bar{3}$. The grain size decreased slightly as Sb concentration increased; whereas the dielectric permittivity of the ceramics increased slightly. The giant dielectric response was considered to be closely related with a reduction in the potential barrier height at grain boundaries (GBs). The activation energy for the dc conduction process is comparable to that for conduction at GBs, indicating that the dc conduction process is associated with the electrical response of GBs.

1 Introduction

$CaCu_3Ti_4O_{12}$ (CCTO) has been attracted considerable attention due to its colossal dielectric constant (ε') of more than 10^4 and stable electrical response over a wide temperature range (100–600 K) [1, 2]. It is theorized to be a kind of potential materials for many electronic technological applications, such as capacitors, memories, gas sensors and filters [3]. CCTO exhibits non-ferroelectric cubic perovskite structure, and no phase or crystal structure transformation occurs below 100 K [4]. Researchers have proposed some possible mechanisms based on extrinsic or intrinsic effects to clarify the origin of unusual dielectric responses, including the local dipole moments associating with off-center displacement of Ti ions [5], the Cu deficiency model [6], the internal domains model [7], and the nanoscale disorder model [8]. The most widely accepted mechanism is the internal barrier layer capacitor (IBLC) model based on Maxwell–Wagner polarization, which states the giant dielectric permittivity should be attributed to the special electrically heterogeneous microstructure [9, 10]. It is consisting of thin insulating grain boundaries (GBs) and large n-type semiconducting grains. The changes in electric conduction of grain, domain boundaries and sample-electrode interface have a notable effect on the dielectric properties [11]. Unfortunately, to date, the comprehensive and accurate mechanism is still controversial.

It is well understood the excellent dielectric response may be derived from the different electric characteristics of grains and GBs. The semiconduction of grains is generated by the oxygen vacancies or non-stoichiometry of Ti and Cu ions as previous reported, implying a promising way to develop new dielectric materials [12, 13]. There are many investigations focusing on the influence of external element doping on CCTO ceramics because the intrinsic electric properties can be tuned. For instance, the effect of substitution of La, Bi and rare-earth element on Ca sites [14–16]; Mn, Mg, Zn on Cu sites [17–19]; Ta, Nb and W on Ti sites [20–22] have been widely studied. Besides the sintering process factors (i.e. sintering temperature and atmosphere), the microstructures and dielectric properties are also significantly influenced by doping metal ions. Unfortunately, up to date, the dielectric properties of Sb-doped CCTO ceramics have not been reported. In this work, we prepared polycrystalline $CaCu_3Ti_{4-x}Sb_xO_{12}$ ceramics (x = 0, 0.025,

Y. Liu (✉) · X. Zhao
School of Chemistry and Environment Engineering, Shaoguan University, Shaoguan 512005, People's Republic of China
e-mail: jackboton@gmail.com

Q. Chen
School of Foreign Languages, Shaoguan University, Shaoguan 512005, People's Republic of China

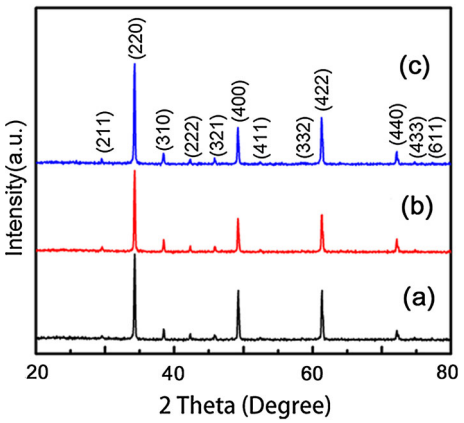

Fig. 1 XRD patterns of *a* CCTO; *b* CCTSbO-1; *c* CCTSbO-2 ceramics prepared at 1,100 °C

0.050) by the conventional solid state reaction method. The purpose was to discuss the role of Sb substitution on dielectric response over wide ranges of temperature and frequency, and the possible mechanism was discussed.

2 Experimental

The $CaCu_3Ti_{4-x}Sb_xO_{12}$ ceramics, where x = 0, 0.025, 0.050, were prepared by the conventional solid state reaction method. The materials are named as CCTO, CCTSbO-1 and CCTSbO-2 respectively. $CaCO_3$ (99.99 % purity), CuO (99 % purity), TiO_2 (99.99 % purity) and Sb_2O_5 (99.99 % purity) were used as starting raw materials. The stoichiometric mixture of the starting raw materials was ball-milled in polytef jar with the ethanol for 24 h. The slurries were dried and then calcined at 950 °C for 10 h. Then, the calcined powders were grinded and pressed into pellets of 10 mm in diameter and ~1 mm in thickness by cooling isostatic pressing at 200 MPa for 2 min. Finally, the pellets were sintered at 1,100 °C for 8 h in muffle furnace, and then cooled to room temperature naturally.

The phase purity and lattice parameter were analyzed by X-ray diffraction (XRD) (MiniFlex-II, Rigaku). Scanning electron microscope (SEM) coupled with Energy dispersive spectroscopy (EDS) (TM3000, HITACHI) was performed to characterize the microstructures and phase formation of the sintered $CaCu_3Ti_{4-x}Sb_xO_{12}$ ceramics. The electric and dielectric properties were measured using an Agilent 4284A LCR Meter in the frequency range of 10^2–10^6 Hz and an oscillation voltage of 1.0 V. The measurements were performed at temperatures ranging from 300 to 480 K. Prior to measurements, the ceramic samples were polished. Silver paint was coated onto both faces of the pellets, and fired at 500 °C for 1 h.

3 Results and discussion

X-ray diffraction (XRD) patterns of $CaCu_3Ti_{4-x}Sb_xO_{12}$ ceramics are shown in Fig. 1. All diffraction peaks for all of the samples confirm the pure formation of the CCTO phase. These XRD patterns can be indexed to a body-centered cubic structure in space group $Im\bar{3}$ (JCPDS Card No.75-2188). Lattice parameters calculated from the XRD patterns using Cohen's least mean square method were found to be 7.394, 7.391 and 7.389 Å for the CCTO, CCTSbO-1 and CCTSbO-2 respectively, which are very close to the value in the literature (7.391 Å) [1]. The slight decrease in lattice parameter with the Sb^{5+} concentration might be ascribed to the smaller ionic radius of Sb^{5+} ($r_6 = 0.600$ Å) than Ti^{4+} ($r_6 = 0.605$ Å) [23].

Figure 2a–c shows the surface morphologies of the sintered $CaCu_3Ti_{4-x}Sb_xO_{12}$ ceramics. The main grain sizes of the CCTO, CCTSbO-1 and CCTSbO-2 ceramic samples were found to be about 42, 30 and 20 μm respectively, which indicates Sb^{5+} ions doping have a significant influence on the microstructures. For CCTO related ceramics, the presence of liquid phase plays an important role in enhancing the grain growth process [12, 20]. Smaller grains of Sb-doped CCTO ceramics may be attributed to the ability of Sb^{5+} to inhibit the growth rate. Figure 3a and b show EDS spectra detected at grain and GBs for the CCTSbO-2 ceramic. The Sb peak was detected in the grain region, confirming the existence of Sb inside grains. It is discovered the relative high Cu peak at the measuring point (2), indicating that CuO phase should be rich in the regions.

Figure 4 illustrates the frequency dependence of dielectric properties for pure and Sb-doped CCTO ceramics at room temperature (300 K). Giant ε' values (~10^4) are exhibited in a broad frequency range, and increase with increasing Sb concentration. The dielectric losses (tan δ) at room temperature for the sintered $CaCu_3Ti_{4-x}Sb_xO_{12}$ ceramics are also simultaneously emerged in Fig. 4. It can be seen that tan δ of the CCTO ceramic is nearly frequency-independent in the frequency range of 10^2–10^5 Hz. While the measuring frequency decreases below 10^3 Hz, tan δ of Sb-doped ceramics increases rapidly. The values of tan δ at 100 Hz were 0.217, 0.941 and 1.480 for CCTO, CCTSbO-1 and CCTSbO-2 respectively, revealing a relaxation process originated from reduction in the intensity of interfacial polarization at GBs [20].

Figure 5a presents the frequency dependence of ε' at different temperatures for the CCTSbO-1 ceramic. At low temperature (<70 °C), ε' depends slightly on frequency from 10^2 to 10^5 Hz. However, when the temperature is increasing, ε' increases and strongly depends on frequency, especially in low-frequency range. Similar trend is observed in tan δ, as shown in Fig. 5b. The dielectric

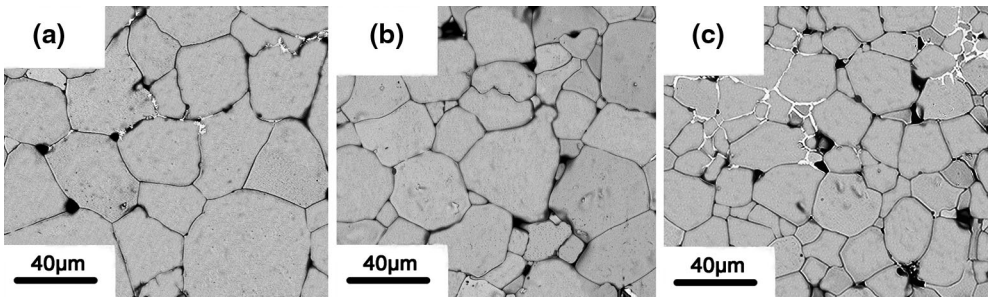

Fig. 2 Surface morphologies of **a** CCTO; **b** CCTSbO-1; **c** CCTSbO-2 ceramics sintered at 1,100 °C

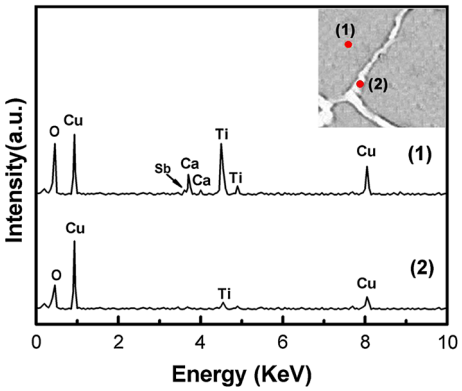

Fig. 3 EDS spectrum of the CCTSbO-2 ceramic detected at *1* grain and *2* GB regions

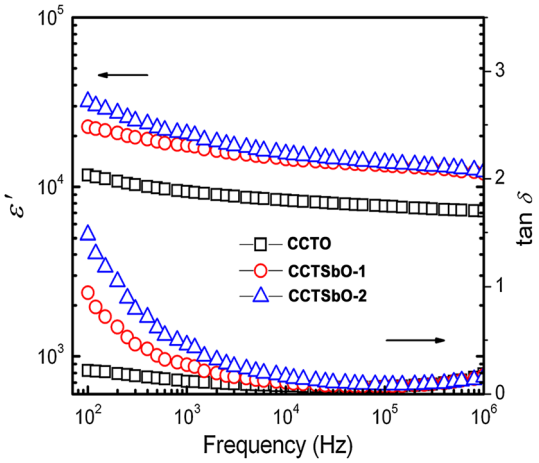

Fig. 4 Dielectric dispersion spectra of $CaCu_3Ti_{4-x}Sb_xO_{12}$ ceramics measured at room temperature

behavior of the sintered $CaCu_3Ti_{4-x}Sb_xO_{12}$ ceramics (especially at high temperature) can be explained by Maxwell–Wagner effect, which is widely adopted to describe the dielectric relaxation behavior of materials with heterogeneous microstructures (e.g., insulating grain with semiconducting GB) [9, 10, 24]. As mentioned above, the

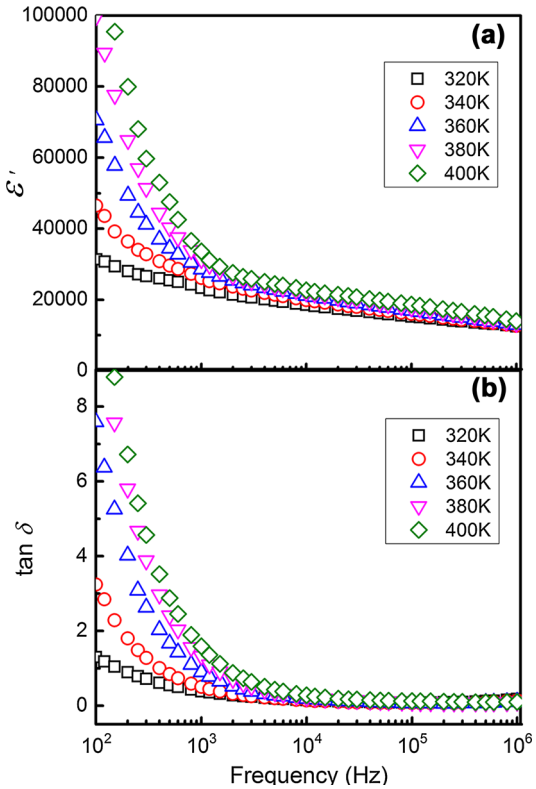

Fig. 5 Frequency dependence of **a** ε' and **b** tan δ at different temperatures for the CCTSbO-1 ceramic

GB region is Cu-rich. Therefore, the dielectric behavior of the sintered $CaCu_3Ti_{4-x}Sb_xO_{12}$ ceramics coincides with this special heterogeneous microstructure.

In order to expound the electric transport mechanism of the $CaCu_3Ti_{4-x}Sb_xO_{12}$ ceramics, the modulus spectroscopy was studied. Typical modulus approaches for the CCTSbO-2 ceramic at a few temperatures showing a broad peak are illustrated in Fig. 6. It can be seen the M'' peak shifts to the high frequency side as temperature increases, indicating a thermal activated dielectric relaxation process. The relaxation time τ is determined as $\tau = 1/2\pi f$, where f is the peak frequency. Inset of Fig. 6 demonstrates the plots of $In(\tau)$ versus $1{,}000/T$ for the sintered $CaCu_3Ti_{4-x}Sb_xO_{12}$ ceramics. The activation energies of the dielectric

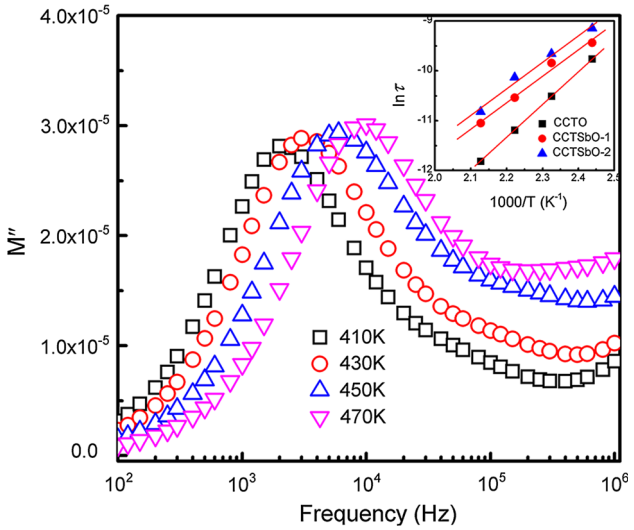

Fig. 6 Typical modulus approaches for the CCTSbO-2 ceramic at a few temperatures; *Inset* presents variation of relaxation time τ with inverse of temperature

relaxations can be described by the following relationship [15, 17, 22]:

$$\tau = \tau_0 \exp\left(\frac{E_a}{K_B T}\right) \quad (1)$$

where τ is the dielectric relaxation time, τ_0 is the pre-exponential factor, and E_a is the activation energies. The values of E_a were calculated to be 0.568, 0.457 and 0.454 eV, and it is notable the E_a of the $CaCu_3Ti_{4-x}Sb_xO_{12}$ ceramics decreases significantly by substitution of Sb^{5+} ions.

It is apparently accepted that the IBLC effect based on Maxwell–Wagner polarization can explain the giant ε' in CCTO-related ceramics. Generally, the related electrical properties of grain and GB in such materials are estimated by an impedance spectroscopy. The grain resistance (R_g) and GB resistance (R_{gb}) at particular temperatures can be determined by the diameter of two semicircular arcs at high and low frequency ranges respectively [10, 12]. Figure 7a provides the impedance complex plane plots for the sintered $CaCu_3Ti_{4-x}Sb_xO_{12}$ ceramics at room temperature. Obviously, only a semicircular arc is observed in the measured frequency range (10^2–10^6 Hz), and the value of a nonzero intercept at high frequencies is very small, indicating the total resistance of the $CaCu_3Ti_{4-x}Sb_xO_{12}$ ceramics is governed by R_{gb} [24]. It is demonstrated R_{gb} trends to decrease with increasing Sb^{5+} concentration, indicating Sb dopant plays an important role in regulating the dielectric properties. The impedance spectrum of the CCTSbO-1 ceramic at different measuring temperatures is presented in Fig. 7b. It is concluded from the expected diameter of a semicircular arc that the value of R_{gb} decreases with increasing temperature, and presents 3–4 orders of magnitude larger than that of R_g. In other words, the dielectric properties are mainly determined by the electrical response at GBs.

According to the IBLC effect, an equivalent circuit model has been considered to analyse the electric properties. The model contains two parallel RC elements (R_gC_g, $R_{gb}C_{gb}$). The element R_gC_g describes the characteristics of grains, while the element $R_{gb}C_{gb}$ delineates the effect caused by GBs (C_{gb} and C_g are the capacitors of GB and grain, respectively) [25]. It has been studied the giant ε' of CCTO related ceramics is concerned with its C_{gb}, and independent of mean grain size [26]. C_{gb} of CCTO-related ceramics is given by $C_{gb} = \sqrt{\varepsilon' q N_d / 8\Phi_b}$, where ε' is the relative permittivity, q is the electronic charge, N_d is the charge carrier concentration in the grains, and Φ_b is the potential barrier height at GBs [27]. From inset of Fig. 7a, the R_g values of all $CaCu_3Ti_{4-x}Sb_xO_{12}$ ceramics are nearly the same, signifying N_d keeps constant. In absence of dc bias, Φ_b is expressed as [27]

$$\Phi_b = \frac{qN_s^2}{8\varepsilon_0 \varepsilon' N_d} \quad (2)$$

where N_s is the acceptor (surface charge) concentration. The decrease in N_s might cause the enhancement of C_{gb}, and ε' increases. It is proposed the positive charge of the supervalent cations (e.g., Nd^{5+}, Ta^{5+} or W^{6+}) in CCTO related ceramics can make compensation of the negative charge of acceptors at GBs and greatly reduce the Φ_b, revealing an increase in ε' as the Sb^{5+} concentration increases [28].

In the IBLC model, the complex impedance (Z^*) can be used to further investigate the electric properties of GBs, which can be expressed as [10, 29],

$$Z(\omega) = \frac{R_g}{1 + i\omega R_g C_g} + \frac{R_{gb}}{1 + i\omega R_{gb} C_{gb}} \quad (3)$$

Accordingly,

$$Z' = \frac{R_g}{1 + (\omega R_g C_g)^2} + \frac{R_{gb}}{1 + (\omega R_{gb} C_{gb})^2} \quad (3-1)$$

and

$$Z'' = R_g\left[\frac{\omega R_g C_g}{1 + (\omega R_g C_g)^2}\right] + R_{gb}\left[\frac{\omega R_{gb} C_{gb}}{1 + (\omega R_{gb} C_{gb})^2}\right] \quad (3-2)$$

Figure 8 reveals the frequency dependence of the imaginary part (Z'') of Z^* at different temperatures for the CCTSbO-2 ceramic. With increasing temperature, the peak position of Z'' shifts to higher frequency and the peak intensity decreases, implying a thermally activated electrical

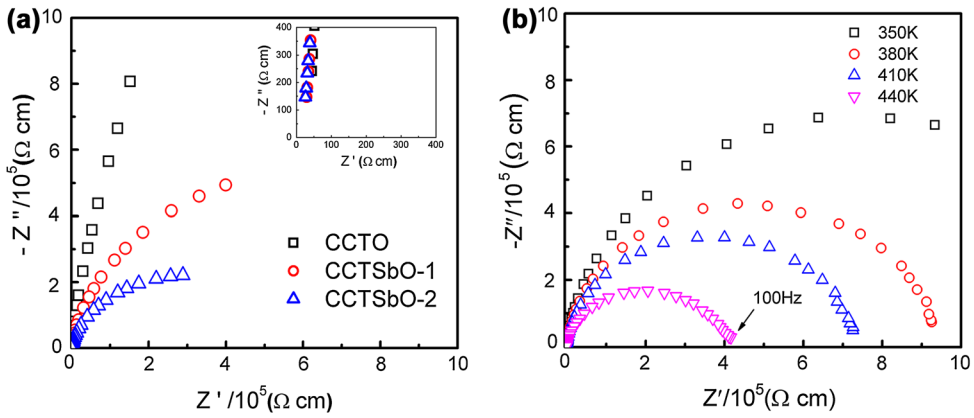

Fig. 7 **a** Impedance complex plane plots for $CaCu_3Ti_{4-x}Sb_xO_{12}$ ceramics at room temperature; *Inset* shows an expanded view of the high frequency data close to the origin. **b** The impedance spectrum of the CCTSbO-1 ceramic at different measuring temperatures

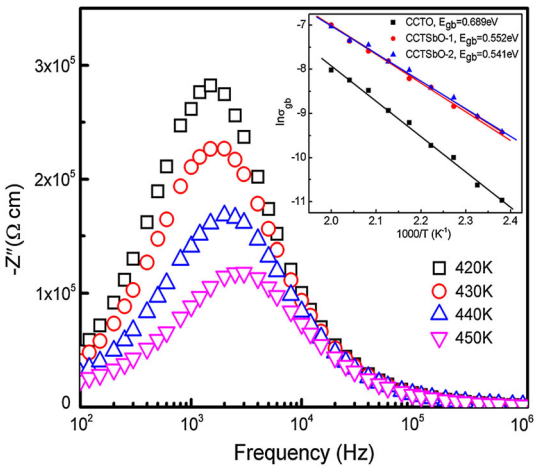

Fig. 8 Frequency dependence of Z'' at different temperatures for the CCTSbO-2 ceramic; *Inset* shows Arrhenius plot of σ_{gb} for $CaCu_3Ti_{4-x}Sb_xO_{12}$ ceramics

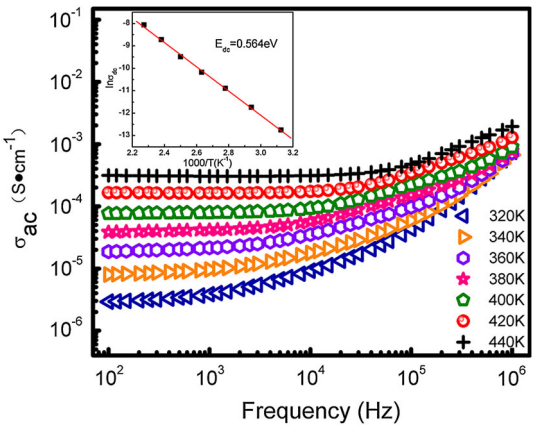

Fig. 9 Frequency dependence of σ_{ac} at different temperatures for the CCTSbO-1 ceramic; *Inset* shows Arrhenius plot of σ_{dc}

response corresponds to a decrease in the value of R_{gb} with increasing temperature [24]. It is known that $R = 2\,Z''_{max}$, where Z''_{max} is the maximum value of Z''. Therefore, the values of R_{gb} at different temperatures can be calculated. As shown in the inset of Fig. 8, it is found that the GB conductivity, $\sigma_{gb} = 1/R_{gb}$, follows the Arrhenius law [15],

$$\sigma_{gb} = \sigma_0 \exp\left(\frac{-E_{gb}}{k_B T}\right) \tag{4}$$

where σ_0 is the pre-exponential factor, E_{gb} is the activation energy for conduction at GBs, k_B is the Boltzmann constant and T is the absolute temperature. The values of E_{gb} were calculated to be 0.689, 0.552 and 0.541 eV respectively, and it is consistent with a decrease in Φ_b. The temperature dependence of ac conductivity of the CCTSbO-1 ceramic is shown in Fig. 9. Generally, with increasing temperature, σ_{ac} increases and becomes more frequency independent in low frequency range. This indicates the low-frequency σ_{ac} can be approximately equal to σ_{dc}, especially at high temperature [20, 24]. The value of σ_{ac} at 100 Hz was used to estimate the value of σ_{dc}. Inset of Fig. 9 presents a plot of $In(\sigma_{dc})$ as a function of reciprocal temperature ($1/T$). It is obtained that σ_{dc} at different temperatures follows the Arrhenius law [15, 30],

$$\sigma_{dc} = \sigma_0 \exp\left(\frac{-E_{dc}}{k_B T}\right) \tag{5}$$

where E_{dc} is the activation energy for the dc conduction process. The calculated E_{dc} was 0.564 eV, which is comparable to E_{gb} (0.552 eV), indicating the dc conduction process is closely associated with the electrical response of GBs for the $CaCu_3Ti_{4-x}Sb_xO_{12}$ ceramics.

4 Conclusion

A series of the sintered $CaCu_3Ti_{4-x}Sb_xO_{12}$ (x = 0, 0.025, 0.050) ceramics have been successfully fabricated by the conventional solid state method, and their microstructures, dielectric properties were investigated. It is concluded all

ceramics are perovskite-related structure in space group *Im* $\bar{3}$, and exhibit giant dielectric permittivity at 300 K. The impedance spectrum analysis shows R_{gb} decreases with increasing Sb concentration, and E_{gb} is comparable to E_{dc}, indicating the dc conduction process is closely associated with the electrical response of GBs for the $CaCu_{3-}Ti_{4-x}Sb_xO_{12}$ ceramics.

References

1. M.A. Subramanian, D. Li, N. Duan, B.A. Reisner, A.W. Sleight, J. Solid State Chem. **151**, 323 (2000)
2. M.A. Subramanian, A.W. Sleight, Solid State Sci. **4**, 347 (2002)
3. S.Y. Chung, I.D. Kim, S.J.L. Kang, Nat. Mater. **3**, 774 (2004)
4. C.C. Homes, T. Vogt, S.M. Shapiro, S. Wakimoto, A.P. Ramirez, Science **293**, 673 (2001)
5. L. Ni, X.M. Chen, Appl. Phys. Lett. **91**, 122905 (2007)
6. T.T. Fang, L.T. Mei, J. Am. Ceram. Soc. **90**, 638 (2007)
7. T.T. Fang, C.P. Liu, Chem. Mater. **17**, 5167 (2005)
8. J.C. Zheng, A.I. Frenkel, L. Wu, J. Hanson, W. Ku, E.S. Bozin, S.J.L. Billinge, Y. Zhu, Phys. Rev. B **81**, 144203 (2010)
9. J.Q. Huang, H. Zheng, Z.H. Chen, Q. Gao, N. Ma, P.Y. Du, J. Mater. Chem. **19**, 3909 (2009)
10. D.C. Sinclair, T.B. Adams, F.D. Morrison, A.R. West, Appl. Phys. Lett. **80**, 2153 (2002)
11. T.B. Adams, D.C. Sinclair, A.R. West, Adv. Mater. **14**, 1321 (2002)
12. T.B. Adams, D.C. Sinclair, A.R. West, J. Am. Ceram. Soc. **89**, 3129 (2006)
13. J. Li, M.A. Subramanian, H.D. Rosenfeld, C.Y. Jones, B.H. Toby, A.W. Sleight, Chem. Mater. **16**, 5223 (2004)
14. L.F. Xu, P.B. Qi, S.S. Chen, R.L. Wang, C.P. Yang, Mater. Sci. Eng., B **177**, 494 (2012)
15. H.A. Ardakani, M. Alizadeh, R. Amini, M.R. Ghazanfari, Ceram. Int. **38**, 4217 (2012)
16. S. Jesurani, S. Kanagesan, T. Kalaivani, K. Ashok, J. Mater. Sci.: Mater. Electron. **23**, 692 (2012)
17. C.H. Kim, Y.H. Jang, S.J. Seo, C.H. Song, J.Y. Son, Y.S. Yang, J.H. Cho, Phys. Rev. B **85**, 245210 (2012)
18. L. Singh, U.S. Rai, K.D. Mandal, Adv. Appl. Ceram. **111**, 374 (2012)
19. L. Ni, X.M. Chen, Solid State Commun. **149**, 379 (2009)
20. P. Thongbai, J. Jumpatam, T. Yamwong, S. Maensiri, J. Eur. Ceram. Soc. **32**, 2423 (2012)
21. M.A. Sulaiman, S.D. Hutagalung, M.F. Ain, Z.A. Ahmad, J. Alloys Compd. **493**, 486 (2010)
22. P. Thongbai, J. Jumpatam, B. Putasaeng, T. Yamwong, S. Maensiri, J. App. Phys. **112**, 114115 (2012)
23. W.T. Hao, J.L. Zhang, Y.Q. Tan, M.L. Zhao, C.L. Wang, J. Am. Ceram. Soc. **94**, 1067 (2011)
24. Y. Liu, W.C. Wang, J.Q. Huang, F. Tang, C. Zhu, Y.G. Cao, Ceram. Int. **39**, 9201 (2013)
25. S.F. Shao, J.L. Zhang, P. Zheng, W.L. Zhong, C.L. Wang, J. Appl. Phys. **99**, 084106 (2006)
26. R. Schmidt, M.C. Stennett, N.C. Hyatt, J. Pokorny, J. Prado-Gonjal, M. Li, D.C. Sinclair, J. Eur. Ceram. Soc. **32**, 3313 (2012)
27. T.B. Adams, D.C. Sinclair, A.R. West, Phys. Rev. B **73**, 094124 (2002)
28. S.Y. Chung, J.H. Choi, J.K. Choi, Appl. Phys. Lett. **91**, 091912 (2007)
29. W. Somphan, N. Sangwong, T. Yamwong, P. Thongbai, J. Mater. Sci.: Mater. Electron. **23**, 1229 (2012)
30. J.L. Zhang, P. Zheng, C.L. Wang, M.L. Zhao, J.C. Li, J.F. Wang, Appl. Phys. Lett. **87**, 142901 (2005)